THERAPEUTIC ADVANCES in
Neurological Disorders

Original Research

Parkinson's disease or multiple system atrophy: potential separation by quantitative susceptibility mapping

Ther Adv Neurol Disord

2023, Vol. 16: 1–14

DOI: 10.1177/17562864221143834

Franz Marxreiter*, **Vera Lambrecht***, **Angelika Mennecke**, **Jannis Hanspach**, **Jelena Jukic**, **Martin Regensburger**, **Juergen Herrler**, **Alexander German**, **Jan Kassubek**, **Georg Grön**, **Hans-Peter Müller**, **Frederik B. Laun**, **Arnd Dörfler**, **Juergen Winkler** and **Manuel A. Schmidt**

Correspondence to:
Franz Marxreiter
Department of Molecular Neurology, University Hospital Erlangen, Schwabachanlage 6, 91054 Erlangen, Germany.

Center for Rare Diseases, University Hospital Erlangen, Erlangen, Germany.
franz.marxreiter@uk-erlangen.de

Vera Lambrecht
Jelena Jukic
Department of Molecular Neurology, University Hospital Erlangen, Erlangen, Germany

Angelika Mennecke
Arnd Dörfler
Manuel A. Schmidt
Institute of Neuroradiology, University Hospital Erlangen, Erlangen, Germany

Jannis Hanspach
Frederik B. Laun
Institute of Radiology, University Hospital Erlangen, Friedrich-Alexander-Universität Erlangen-Nürnberg (FAU), Erlangen, Germany

Martin Regensburger
Juergen Winkler
Department of Molecular Neurology, University Hospital Erlangen, Erlangen, Germany

Center for Rare Diseases, University Hospital Erlangen, Erlangen, Germany

Juergen Herrler
Alexander German
Institute of Neuroradiology, University Hospital Erlangen, Erlangen, Germany

Institute of Radiology, University Hospital Erlangen, Friedrich-Alexander-Universität Erlangen-Nürnberg (FAU), Erlangen, Germany

Jan Kassubek
Hans-Peter Müller
Department of Neurology, Ulm University, Ulm, Germany

Abstract

Background: Due to the absence of robust biomarkers, and the low sensitivity and specificity of routine imaging techniques, the differential diagnosis between Parkinson's disease (PD) and multiple system atrophy (MSA) is challenging. High-field magnetic resonance imaging (MRI) opened up new possibilities regarding the analysis of pathological alterations associated with neurodegenerative processes. Recently, we have shown that quantitative susceptibility mapping (QSM) enables visualization and quantification of two major histopathologic hallmarks observed in MSA: reduced myelin density and iron accumulation in the basal ganglia of a transgenic murine model of MSA. It is therefore emerging as a promising imaging modality on the differential diagnosis of Parkinsonian syndromes.

Objectives: To assess QSM on high-field MRI for the differential diagnosis of PD and MSA.

Methods: We assessed 23 patients (nine PDs and 14 MSAs) and nine controls using QSM on 3T and 7T MRI scanners at two academic centers.

Results: We observed increased susceptibility in MSA at 3T in prototypical subcortical and brainstem regions. Susceptibility measures of putamen, pallidum, and substantia nigra reached excellent diagnostic accuracy to separate both synucleinopathies. Increase toward 100% sensitivity and specificity was achieved using 7T MRI in a subset of patients. Magnetic susceptibility correlated with age in all groups, but not with disease duration in MSA. Sensitivity and specificity were particularly high for possible MSA, and reached 100% in the putamen.

Conclusion: Putaminal susceptibility measures, in particular on ultra-high-field MRI, may distinguish MSA patients from both, PD and controls, allowing an early and sensitive diagnosis of MSA.

Keywords: high-field magnetic resonance imaging, iron, multiple system atrophy, Parkinson's disease, quantitative susceptibility mapping

Received: 11 April 2022; revised manuscript accepted: 8 November 2022.

Introduction

Multiple system atrophy (MSA) is a rare, rapidly progressing oligodendroglial synucleinopathy. The course of MSA is characterized by a mean survival of less than 10 years after symptom onset.[1,2] Clinically, two distinct MSA subtypes are classified based on the prevailing motor phenotype: MSA-p features predominant Parkinsonism, while MSA-c shows prominent cerebellar ataxia. Both phenotypes present with an early and severe autonomic failure.[3] While a definite diagnosis of MSA requires post mortal neuropathological confirmation, clinical consensus criteria have been established, defining possible and probable MSA.[3] Yet,

Georg Grön
Department of Psychiatry and Psychotherapy III, Ulm University, Ulm, Germany
*equal contribution.

there is currently no reliable biomarker allowing the lifetime diagnosis of MSA or the differential diagnosis of MSA and Parkinson's disease (PD). Therefore, a recent view point on the second consensus criteria for MSA stressed the urgent need for improved neuroradiologic biomarkers.[4]

Routine cerebral magnetic resonance imaging (MRI) has been extensively studied in Parkinsonian syndromes and is primarily recommended to exclude secondary causes of Parkinsonism. In addition, high-field and ultra-high-field MRI is being studied in PD and atypical Parkinsonism.[5] In MSA, putaminal hypointensity and hyperintense rim, pontine, and cerebellar vermis atrophy, as well as signal changes in the pons or middle cerebellar peduncle, including the 'hot-cross bun' sign, are observed at intermediate and advanced disease stages.[6] These changes lack sensitivity for the differential diagnosis of MSA, in particular at early disease stages. Various studies using routine MRI or susceptibility-weighted images (SWIs), reliably differentiated PD from healthy controls, based on the loss of nigral hyperintensity, known as swallow tail sign. However, studies using routine MRI sequences or SWI as a stand-alone protocol were not able to distinguish between PD and MSA, using neither 3T nor 7T MRI scanners.[7,8] These studies predominantly focused on the structural pattern of the substantia nigra (SN), but neuropathological changes in MSA are more widespread, affecting in particular extranigral structures like the striatonigral and olivopontocerebellar system in MSA-p and MSA-c, respectively.[9] Especially within the putamen (Pu), myelin loss and iron deposition are two of the most prominent neuropathological hallmarks of MSA.[10–12]

Quantitative susceptibility mapping (QSM) is able to asses iron accumulation and demyelination *in vivo*.[13] Magnetic susceptibility represents an intrinsic tissue property that is predominantly associated with iron levels, but to a certain extent also with myelin density. Using a series of complex post-processing techniques, phase maps of gradient echo MRI are processed to estimate the spatial distribution of tissue magnetic susceptibility.[14] As recently demonstrated, magnetic susceptibility correlates both with tissue iron levels and myelin density, reaching an excellent specificity and sensitivity in differentiating between transgenic MSA mice (MBP29) and control littermates.[13]

Recent proof of concept studies evaluated QSM as stand-alone MRI modality for the diagnosis of PD,[15] and also for the differential diagnosis of atypical Parkinsonian syndromes, already providing promising results for striatal and nigral susceptibility.[16–18] In the present two-center study (University Hospitals Erlangen and Ulm, Germany), QSM was investigated as imaging modality for the differential diagnosis of PD and MSA. Participants were imaged using a 3T MRI scanner, including a subset of participants undergoing subsequent 7T MRI. In particular, magnetic susceptibility values of different prototypically affected brain regions [Pu, pallidum (GP), SN, red nucleus (RN), and dentate nucleus (DN)] were compared among PD, MSA patients, and controls. Moreover, correlations of magnetic susceptibility with covariates influencing QSM, such as age, and also important clinical characteristics, such as disease duration and severity of motor symptoms were performed.

Materials and methods

Clinical phenotyping

PD patients were diagnosed according to current consensus criteria.[19] Healthy controls did not present with prodromal symptoms suggestive of PD.[20] MSA was diagnosed as possible and probable MSA and classified as MSA-p or MSA-c, according to the present consensus criteria.[3] Motor symptoms were rated according to the Unified Parkinson's Disease Rating Scale (UPDRS) part III.[21] Disease severity was staged using the Hoehn and Yahr scale (H + Y).[22]

Image post-processing

Using two different 3T MRI scanners, 3T MRI data were acquired from the same vendor (Magnetom Trio and Magnetom Prisma, Siemens Healthcare GmbH, Erlangen, Germany) using a 1Tx32Rx Head coil. Using a 7T whole-body MR system (Magnetom Terra, Siemens Healthcare GmbH, Erlangen, Germany), 7T MRI data were acquired with an 8Tx/32Rx head coil (Nova Medical, Wilmington, MA, USA). At the 7T MR scanner, a 3D T1 magnetization prepared rapid gradient echo (MPRAGE) scan with fast online customized (FOCUS) parallel transmit pulses[23] was performed for anatomical information. The acquisition parameters were: repetition time (TR) 3 s, echo time (TE) 3.37 ms, flip angle 7°, isotropic voxel size of 0.65 mm, 256 sagittal slices with the

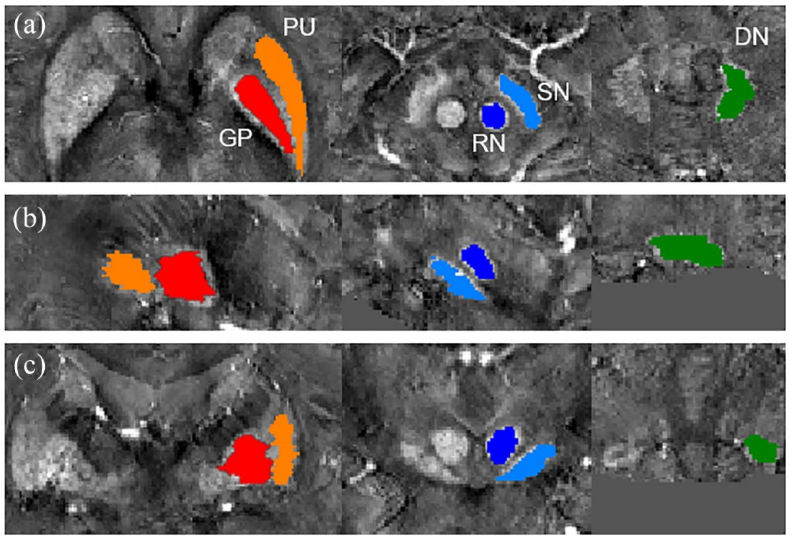

Figure 1. Overview of segmented volumes of interest (VoIs). Axial (a), sagittal (b), and coronal (c) susceptibility maps at 3T displaying the putamen (Pu) and the pallidum (GP) at the level of the foramen of Monroi, the red nucleus (RN), and substantia nigra (SN) at the level of the maximal diameter of the RN, as well as the cerebellar VoI: dentate nucleus (DN).

matrix 336 × 384, and time of acquisition (TA) 5:46 min. For QSM, a gradient echo sequence (GRE) with ASPIRE coil combination was applied.[24] At 7T, five TEs of 5/10/15/20/25 ms and a TR of 30 ms were used with two nominal image resolutions, Res1: 256 slices with field of view (FoV) 182 × 182 mm², acquisition matrix 304 × 304, voxel size 0.6 × 0.6 × 0.6 mm³, acquisition time 7:36 min, and Res2: 256 slices with FoV 180 × 180 mm², acquisition matrix 256 × 256, voxel size 0.7 × 0.7 × 0.7 mm³, acquisition time 6:25 min. Due to a prolonged transverse relaxation time and lower signal to noise ratio at 3T, we measured with a larger number of echoes and a larger voxel size at the lower magnetic field strength. On both 3T machines, 11 TE equidistantly distributed between 5 and 55 ms and a TR of 60 ms were used with the resolution Res3: 176 slices with FoV 192 × 192 mm² with acquisition matrix 192 × 192, resulting in a voxel size of 1 × 1 × 1 mm³, acquisition time 6:50 min. All measurements were done with a flip angle of 15° and PAT-factor 4 (GRAPPA 2 and 3D slice acceleration 2)

Data processing

Susceptibility maps were generated after performing the following post-processing steps. Phase maps were unwrapped applying a Laplacian-based phase unwrapping algorithm.[25] Using the brain extraction tool created by Isensee *et al.*[26] a brain mask was generated based on the magnitude images. The background field was removed by the sophisticated harmonic artifact reduction for phase data (V-SHARP) with varying spherical kernel sizes.[27] The individual susceptibility maps for each echo were calculated with iLSQR. At last, one final susceptibility map was generated as the weighted average of the single echo susceptibility maps, weighted with the squared TE and the squared signal magnitude.[28,29] Susceptibility maps were referenced to the brain average susceptibility value.

Ten brain regions (five per hemisphere) of interest [volumes of interest (VoIs)] were manually segmented on a subject-by-subject basis in the QSM data sets as shown in Figure 1 using the Medical Imaging Toolkit [MITK, German Cancer Research Center (DKFZ), Heidelberg, Germany, www.mitk.org]. The VoIs were DN, SN, RN, GP, Pu, right, and left, respectively. All VoIs were manually segmented, covering all related slices of the corresponding anatomical structure, in the 3T susceptibility maps in axial orientation by taking into account sagittal and coronal view, resulting in 3D VoIs (Figure 1). Seven-Tesla susceptibility maps were rigidly registered to the 3T susceptibility maps using FSL FMRIB's Linear Image Registration Tool (FLIRT). VoIs were transformed using the

Table 1. Overview of demographic and clinical characteristics of the study population, receiving 3T MRI.

	PD	MSA	ctrl
n	9	14	9
		10 (probable MSA)	
		4 (possible MSA)	
Age (years)	60.8 ± 8.6	63.3 ± 10.1	54.22 ± 3.8
gender (%male)	66.7	35.7*	66.7
disease duration (years)	6.0 ± 5.8	4.0 ± 1.3	
UPDRS-III	12.7 ± 9.5	34.9 ± 9.2***	
UMSARS-I		18.9 ± 5.5	
UMSARS-II		21.1 ± 6.5	
H + Y	1.68 ± 0.56	4.00 ± 0.76***	

H + Y, Hoehn and Yahr; MRI, magnetic resonance imaging; MSA, multiple system atrophy; PD, Parkinson's disease; UMSARS, Unified Multiple System Atrophy Rating Scale; UPDRS, Unified Parkinson's Disease Rating Scale.
***$p < 0.001$; *$p < 0.05$.

transformation matrices generated by the registration and subsequently, if needed, manually corrected.[30,31] The mean and standard deviation of the susceptibility values were calculated within each VoI. Finally, for each participant, the mean susceptibility of the right and left hemispheres was calculated and used for statistical analysis.

Statistics

All clinical data were stored within a Microsoft Access database and exported as .xlsx files for analysis. Data completeness was assessed using Microsoft Excel(C). Subsequent statistical analysis was performed using R Studio (C) (Version 1.3.1093). First, data were examined for normality distribution using a Shapiro–Wilk's test. In case of normal distribution, data were analyzed using a Welch's *t*-test or analysis of variance (ANOVA). In case the assumption of normality was violated, a Wilcoxon rank-sum test was applied. In all cases, *post hoc* testing was performed with Bonferroni correction for multiple comparisons. Categorical variables were analyzed using a chi-square test. Receiver-operating characteristic (ROC) curves and Youden indices were applied to assess the specificity and sensitivity to differentiate PD from MSA. Correlations of clinical variables with susceptibility values were analyzed using Pearson's correlation coefficient.

Results

Subjects and clinical assessment

PD patients ($n = 9$), MSA patients ($n = 14$), and healthy controls (ctrl: $n = 9$) were recruited from the movement disorder outpatient centers at the University Hospital Erlangen and Ulm. Of 14 MSA patients, 10 were diagnosed with probable, four with possible MSA. Furthermore, MSA patients were categorized as MSA-p ($n = 7$) or MSA-c ($n = 7$). Demographics and basic clinical information are summarized in Table 1. In summary, despite similar disease duration (*t*-test, $p > 0.05$), MSA patients were significantly more affected as evidenced by higher UPDRS-III and H + Y scores. In addition, the examined MSA cohort consisted of significantly fewer male participants than the PD group (for details, see Table 1).

Increased putaminal and nigral susceptibility in MSA compared with PD and controls

Using ANOVA with Bonferroni *post hoc* testing, mean susceptibility values significantly differed

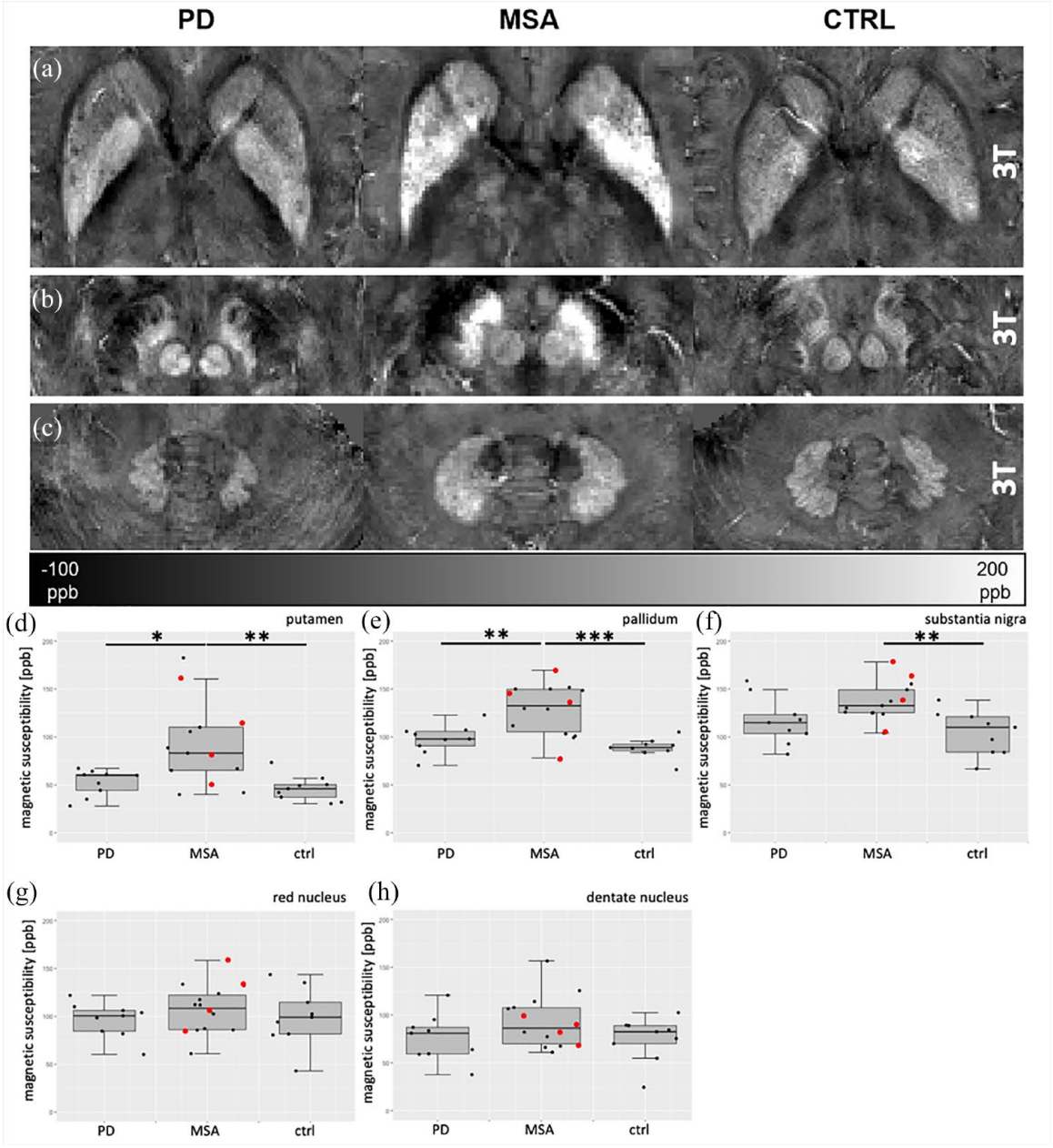

Figure 2. Group comparisons of magnetic susceptibility within different brain regions at 3T. (2a–c) Representative axial susceptibility maps at 3T derived from PD, MSA, and controls (ctrl) for each axial level analyzed. Differences between groups are shown in 2d–h. Red dots indicate possible MSA patients.
ANOVA, *post hoc* testing: Bonferroni); ppb, parts per billion.
*$p < 0.05$, **$p < 0.01$, *** $p < 0.001$.

between PD and MSA, and between controls and MSA in all VoIs examined, apart from the DN and the RN. Susceptibility values were significantly increased in MSA in the GP (PD *versus* MSA: $p = 0.00320$; MSA *versus* ctrls: $p = 0.00017$), and the Pu (MSA *versus* PD: $p = 0.0128$; MSA *versus* ctrl: $p = 0.0046$). A difference in mean susceptibility was observed between controls and MSA in the SN (MSA *versus* ctrl: $p = 0.0038$) using 3T MRI. For details, see Figure 2.

QSM separates MSA from PD reaching high sensitivity and specificity

To further delineate the ability of QSM to differentiate MSA from PD at 3T MRI, we examined

Table 2. Susceptibility values of the PD and the MSA groups.

	PD	MSA	*p*-value
GP	97.65 ± 14.98	128.77 ± 26.25	0.00168
Pu	52.39 ± 13.74	99.46 ± 50.86	0.0048
RN	96.4 ± 18.3	107.24 ± 25.41	0.2481
SN	116.64 ± 24.83	142.53 ± 26.40	0.028
DN	76.5 ± 24.4	93.22 ± 27.1	0.141

Data are presented as mean ± *SD* (in parts per billion) of the PD and the MSA group, and *p*-values for group comparison using a *Welch's t-test.*
MSA, multiple system atrophy; PD, Parkinson's disease.

mean susceptibility values, separately between both groups, using a Welch's *t*-test (see Table 2). A significant increase of magnetic susceptibility in the MSA group was observed within the GP, Pu, and SN compared with PD. Subsequently, we applied ROC curve analysis to assess the sensitivity and specificity for QSM to differentiate between PD and MSA for each VoI. To separately capture the performance of each VoI and to develop a criterion for selecting the optimal cut-off point, Youden's J statistic was calculated. The GP and the Pu showed the highest diagnostic accuracy with an area under the curve (AUC) of 0.841 and 0.825, respectively. Using a cut-off of 126 parts per billion (ppb) in the GP, 100% sensitivity and 64% specificity to discriminate between MSA and PD is achieved. Furthermore, MSA is diagnosed with a sensitivity of 89% and a specificity of 79% based on putaminal QSM [Figure 3(a)].

Within the MSA cohort, four patients were classified as possible MSA (displayed in red in Figure 2). When comparing possible and probable MSA patients with PD using ANOVA, we observed significantly larger susceptibility values in possible MSA compared with PD in the GP ($p < 0.05$; Figure 4). Using ROC analysis, QSM was able to identify possible MSA patients in the GP, Pu, and SN with 100%, and 78% sensitivity, and 75% specificity, respectively (Figure 3B).

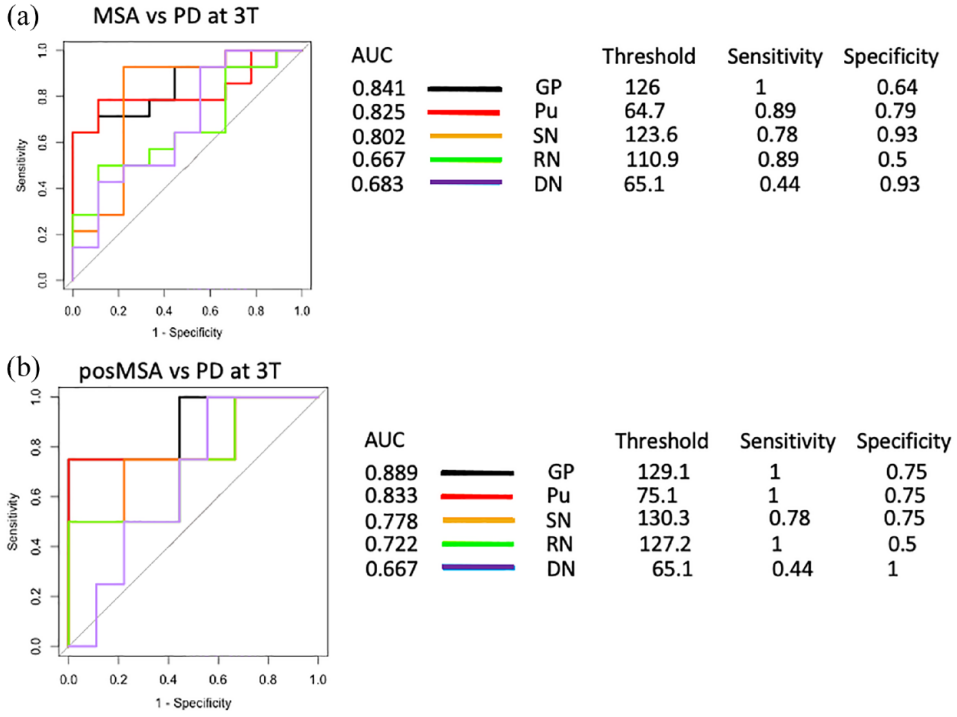

Figure 3. QSM separates PD from MSA at 3T. ROC analysis of magnetic susceptibility values for the differential diagnosis of (a) MSA *versus* PD and (b) possible MSA (posMSA) *versus* PD. Thresholds were derived using Youden indices.
AUC, area under the curve; DN, dentate nucleus; GP, pallidum; Pu, putamen; RN, red nucleus; SN, substantia nigra.

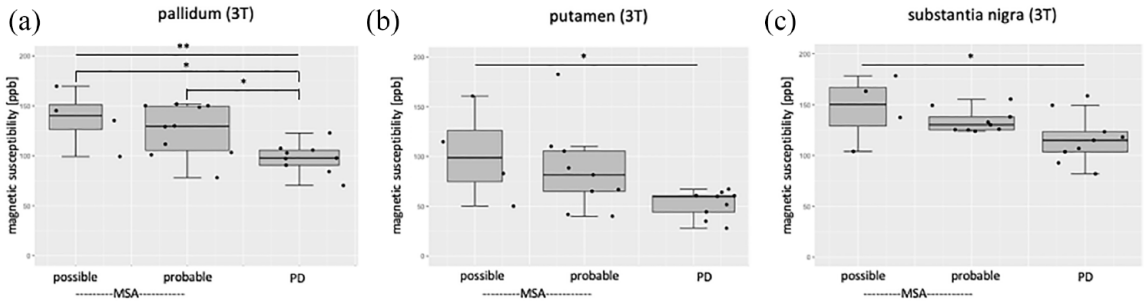

Figure 4. Group comparisons of possible and probable MSA and PD in VoI at 3T within (a) the pallidum, (b) the putamen, and (c) the substantia nigra.
ANOVA, post hoc testing: Bonferroni; ppb, parts per billion.
*$p < 0.05$, **$p < 0.01$, ***$p < 0.001$.

Age and disease duration-dependent impact on QSM in MSA and PD

To evaluate to which extent QSM is influenced by age and covariates like motor impairment and disease duration, we performed a correlation analysis of mean magnetic susceptibility of each VoI of the PD and MSA groups separately for age, UPDRS-III motor score, and disease duration (Figure 5). In summary, significant correlations were observed between age and susceptibility within the RN at 3T, and between UPDRS-II ratings and pallidal as well as nigral susceptibility in MSA patients. In contrast, no significant correlations of disease duration and susceptibility could be observed throughout all VoIs for MSA and PD patients.

7T MRI increases sensitivity and specificity in the differential diagnosis of MSA versus *PD*

To investigate whether higher magnetic field strength increases sensitivity and specificity of QSM for the diagnosis of MSA, a subpopulation was studied on a 7T MRI scanner, in addition to 3T MRI (see Supplementary Figure 2). The demographic characteristics of this subgroup are summarized in Table 3. Only male participants underwent 7T imaging. With respect to H + Y and UPDRS-III, the 7T PD and MSA subgroups showed comparable disease stage and motor impairment as the total study population. At 3T, this subgroup of patients showed an increased sensitivity and specificity compared with the entire 3T population (Supplementary Figure 1 F). At 7T, significant differences between PD and MSA were observed in the GP ($p < 0.05$), Pu ($p < 0.05$), the SN ($p < 0.01$), and DN [$p < 0.01$, Figure 6(a)–(e)]. We used ROC analysis to test the potential of 7T in the differential diagnosis of MSA *versus* PD. We observed an improvement in sensitivity up to 100% on 7T [Figure 6(f), Supplementary Table 1].

Discussion

In this bicentric study, we investigated the potential of QSM for the differential diagnosis of the Parkinsonian syndromes PD *versus* MSA. We show high sensitivity and specificity for 3T MRI, making QSM a highly promising biomarker candidate for the differential diagnosis of PD and MSA, also for patients fulfilling the criteria of possible MSA. In particular, Pu and GP were structures providing the highest sensitivity and specificity. In addition, our data suggest that ultra-high-field MRI may further improve sensitivity (up to 100%) of differential diagnostic classification.

QSM as promising differential diagnostic imaging biomarker

Loss of dopaminergic neurons in the SN is present in sporadic and atypical Parkinsonism, whereas Pu and GP are spared in PD.[9] This neuropathological pattern may account for the results of previously published imaging studies using SWI or QSM, solely assessing the SN.[7,32] As pathological alterations in MSA are much more widespread across the basal ganglia,[9] we additionally focused on extranigral structures, that is, the Pu, GP, RN, and the DN. In MSA, severe glial dysfunction and abundant iron accumulation is present in particular in the Pu and the GP. Accordingly, assessing the iron content using 3T QSM in the Pu, GP, RN, and DN of MSA and PD patients, we observed good to excellent

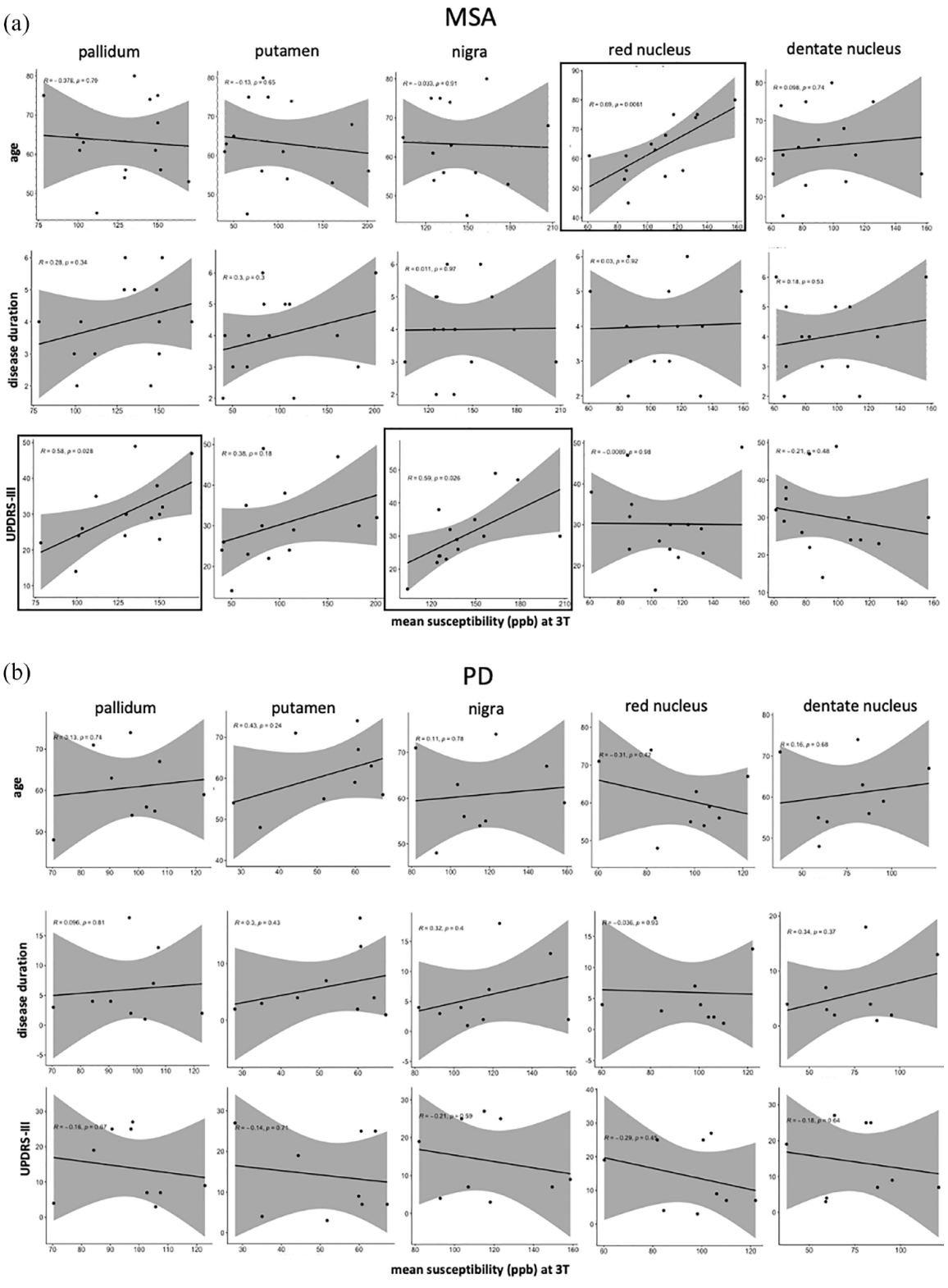

Figure 5. Correlation analysis of demographic and clinical characteristics *versus* magnetic susceptibility in ROIs at 3T in (a) MSA and (b) PD patients.
ppb, parts per billion.

Table 3. Overview of demographic and clinical characteristics of the 7T study population.

	PD	MSA	ctrl
N	8	5	9
age	60.0 ± 8.9	57.0 ± 9.4	54.2 ± 3.8
gender (%male)	75.0	100	66.6
disease duration	5.12 ± 5.51	3.6 ± 0.89	
UPDRS-III	14.9 ± 10.2	30.0 ± 12.3	
H + Y	1.69 ± 0.59	3.4 ± 0.55	

H + Y, Hoehn and Yahr; MSA, multiple system atrophy; PD, Parkinson's disease; UPDRS, Unified Parkinson's Disease Rating Scale.

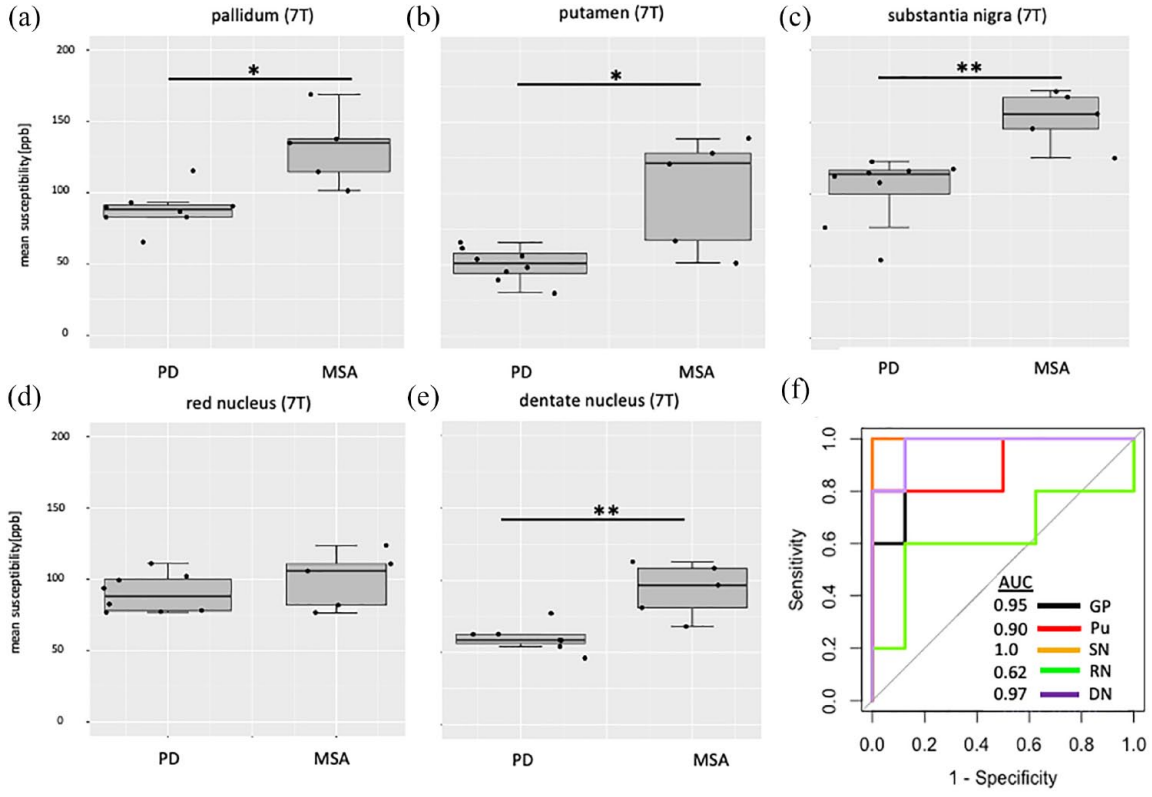

Figure 6. Seven-Tesla MRI increases sensitivity and specificity. (a–e) Group comparisons of magnetic susceptibility at 7T within different brain regions and (f) ROC analysis of 7T study population. High-field imaging at 7T yields increased diagnostic accuracy between PD and MSA. Highest accuracy was recorded for the putamen (Pu) and the substantia nigra (SN) with an area under the curve (AUC) of 1.0 as well as sensitivity and specificity of 100%.

sensitivity and specificity for the differentiation of both synucleinopathies. Particularly, promising results were observed in the Pu reaching up to 90% accuracy, followed by the SN and the RN with 83% and 70% accuracy, respectively. Interestingly, the GP obtained high diagnostic accuracy (AUC: 87%) in the present cohort, while reaching moderate or no significance in previous studies.[16,17] Susceptibility in the SN was not able to distinguish between PD and ctrls, most

likely due to the limited sample size in our study, compared with other studies specifically addressing QSM in the SN of PD *versus* ctrls.[33]

QSM provides high diagnostic accuracy, possibly early in the course of MSA

An early and precise diagnosis of MSA is of essential importance, since otherwise the disease may be already too advanced for therapeutic interventions to be effective.[2] In addition, motor decline appears to be more prominent in earlier disease stages as implied by the more rapid decline in the first year of follow-up in a large European cohort study.[1] In the present small subcohort of possible MSA patients, 3T QSM showed promising results, in particular with excellent sensitivity in the VoIs Pu (82%), GP (100%), and SN (100%), while the specificity ranged between 60% (GP) and 100% (Pu). This suggests that QSM of well-defined VoIs may be particularly valuable in early MSA stages. To qualitatively assess the influence of disease duration, and age on QSM values, we used correlation analysis. As the sample size of the examined cohort is too small for robust correlations, the results must be interpreted with caution. Further studies with higher sample sizes are needed to delineate the effects of these covariates on the differential diagnosis of Parkinsonian syndromes more robustly. Yet, our data suggest that longer disease duration in PD may be associated with increased susceptibility values, whereas magnetic susceptibility in MSA may undergo less changes with disease duration. This further supports the notion that the differential diagnostic potential of QSM to separate MSA from PD is probably higher in early disease stages, since susceptibility values in advanced PD develop toward a range observed in MSA.

The influence of age on QSM values in PD and MSA

Susceptibility values have been reported to increase upon aging.[34] However, the highest increases in magnetic susceptibility upon aging are seen between ages 10 and 40, with little or no further increase beyond the age of 50.[34] Even though our results need to be interpreted with caution, no correlation of age and susceptibility values was observed in the PD and MSA groups. Thus, the influence of age on QSM for the differential diagnosis of PD *versus* MSA may be neglectable. With respect to the differential diagnosis of PD *versus* ctrls, it is noteworthy that studies observing increased QSM in PD mostly examine PD cohorts with a mean age of about 65 years. In younger PD cohorts (average age: 55 years), no differences in SN QSM are observed (for review, see Ravanfar *et al.*).[33] Therefore, it may be that the examined PD cohort here (60.8 years) is too young to observe differences compared with ctrls.

Is QSM a suitable marker for disease progression?

It has not yet been studied if QSM is able to mirror disease progression in MSA. Our MSA group showed great interindividual differences in susceptibility, especially in the striatum, likely reflecting variable interindividual iron load. One may argue that this region is therefore not a promising candidate to detect disease progression. In line, we only observe weak correlation with disease duration in MSA. Taken this into account, a single QSM measurement might not allow to determine the actual disease stage or motor impairment in both, PD and MSA. However, progressive iron accumulation and therewith increasing susceptibility contrast has previously been shown in PD, and may occur in the course of MSA, as well.[35,36] In this regard, one limitation of our study is missing longitudinal data, that would allow addressing these important issues.

Why does 7T MRI yield increased diagnostic accuracy?

The promising results of 3T QSM regarding differentiation of early MSA and PD and the added sensitivity on 7T MRI makes 7T QSM a promising candidate for a reliable differential diagnostic imaging biomarker. While mean susceptibility values at 3T (Supplementary Figure 1) and 7T (Figure 6) were comparable, *SD*s were lower on 7T, most likely accounting for the increase in sensitivity. The larger phase contrast and increased signal-to-noise ratio of 7T MRI compared with lower field strengths most likely account for this observation (see supplementary figure 2). Even though mean susceptibility values at 3T and 7T were comparable (Supplementary Figures 1 and 6), Even though mean susceptibility values at 3T and 7T were comparable (Supplementary Figures 1 and 6), there is a slight deviation. This is probably due to the TE and magnetic field strength dependence described in the literature.[37,38] TEs in

our study at 7T compared with 3T are slightly shorter than the factor 2.6, which is recommended by Lancione *et al.* to maximize reproducibility. Also, to increase the contrast-to-noise ratio (CNR) at 3T, more TEs were acquired at 3T than at 7T due to the longer TR. However, since only comparisons within each field strength were performed in this study, a systemic error due to TE or magnetic field strength dependence is minimized. Nevertheless, this could become a problem in future longitudinal studies, if only measurements at 3T or 7T are available, since the susceptibility values of the patients can then only be compared with each other to a limited extent. In addition, there is a slight difference in voxel size, between the PD (0.6 mm iso) and MSA (0.7 mm iso) cohort. As there is a voxel size dependency of susceptibility, that is, the greater the voxel size, the lower the susceptibility, it is conceivable that the difference between PD and MSA in susceptibility is even larger if the different voxel sizes in the presented data are taken into account.[39]

Study limitations

From a clinical viewpoint, it is noteworthy that, due to physical disabilities of some patients and technical features of the 7T scanner used (e.g. no height-adjustable table, restricted handling of the head coil), some participants could not receive 7T imaging. Nevertheless, the results of the 7T subgroup are promising and suggest that the already excellent differential diagnostic power regarding MSA *versus* PD of the Pu may be further improved by an ultra-high-field scanner. To test the suitability of QSM for the diagnosis of MSA on an individual level, validating the defined cut-off values of this study in an independent cohort is necessary, especially as ROC curve analysis may overestimate diagnostic performance. Using the data derived from this study, an a priori power analysis (using G*Power)[40] suggest an n of 22 per group to be sufficient to detect differences in the SN with a power of 0.9, while for the Pu and the GP, an n of 15 and 12, respectively, would allow to detect differences with a power of 0.9. Thus, the sample size in this study is large enough to deliver robust results for the Pu and the GP at 3T, whereas the results presented for the 7T cohort and the possible MSA subgroup need to be interpreted with caution. A larger multi-center study, increasing the sample size may also allow for more advanced statistical analysis, such as cross-validation approaches. In addition, progressive supranuclear palsy (PSP) is another important differential diagnosis of Parkinsonism also characterized an increased iron load in the striatum. Future studies should include a group of PSP patients to further delineate the ability of QSM imaging to differentiate these disease entities. Furthermore, future studies should aim to include possible MSA patients and provide clinical follow-up information of this cohort to increase diagnostic confidence and strengthen the role of QSM in early differential diagnostic power.

Summary

In conclusion, our study suggests that QSM is a highly promising candidate for a diagnostic imaging biomarker in the classification of Parkinsonian syndromes. The imaging technology to obtain susceptibility maps has already been shown to be stable and well reproducible across multiple scanner systems.[41] Thus, implementation of a protocol with integrated QSM reconstruction should be part of the routine differential diagnostic algorithm of Parkinsonian syndromes. Seven-Tesla QSM has the potential to further increase the already good sensitivity up to 100%. The extent to which longitudinal changes reflect disease progression must be addressed by future longitudinal studies using QSM.

Declarations

Ethics approval and consent to participate

This study was performed according to the Declaration of Helsinki, the European Guidelines for Good Clinical Practice, and in accordance with local legislation (BayKrG Art. 27 (4)). Study approval was granted by the local ethics committees (No.189_15 BNo. 21_20B, FAU Erlangen-Nürnberg, Germany and No. 78/20, Ulm University, Germany) and participants provided written informed consent prior to study procedures.

Consent for publication

Not applicable.

Author contributions

Franz Marxreiter: Conceptualization; Formal analysis; Funding acquisition; Investigation; Project administration; Resources; Supervision; Writing – original draft; Writing – review & editing.

Vera Lambrecht: Conceptualization; Formal analysis; Writing – original draft.

Angelika Mennecke: Data curation; Formal analysis; Methodology; Software; Validation.

Jannis Hanspach: Data curation; Formal analysis; Software; Validation; Visualization; Writing – original draft.

Jelena Jukic: Investigation; Project administration; Resources.

Martin Regensburger: Project administration; Resources; Writing – review & editing.

Juergen Herrler: Data curation; Formal analysis; Resources; Software.

Alexander German: Data curation; Formal analysis.

Jan Kassubek: Methodology; Project administration; Resources; Supervision; Validation; Writing – review & editing.

Georg Grön: Resources; Software; Validation; Writing – review & editing.

Hans-Peter Müller: Data curation; Resources; Validation.

Frederik B. Laun: Conceptualization; Data curation; Formal analysis; Methodology; Writing – original draft; Writing – review & editing.

Arnd Dörfler: Conceptualization; Resources; Software; Supervision.

Juergen Winkler: Conceptualization; Resources; Writing – review & editing.

Manuel A. Schmidt: Conceptualization; Data curation; Formal analysis; Methodology; Project administration; Supervision; Writing – review & editing.

Acknowledgements
The authors thank the participants of the study, as well as Sabine Stallforth, Pia-Marie Pryssok and Patrick Süß for assistance with patient recruitment.

Funding
The authors disclosed receipt of the following financial support for the research, authorship, and/or publication of this article: This study was supported by the ELAN Fund of the Interdisciplinary Center for Clinical Research (IZKF) at the University Hospital of the University of Erlangen-Nürnberg (P076). FM and JW are supported by the 'Forschungsstiftung Medizin' of the University Hospital Erlangen, the Bavarian Research Consortium 'Interaction of Human Brain Cells' (ForInter) which is funded by the Bavarian Ministry of Science and the Arts. JW is funded by the joint project 'Throughput Approaches for the Individualized Therapy of Tau-Related Diseases' (HIT-Tau; 01EK1605B) which is funded by the German Federal Ministry of Education and Research. Funding for the position of FBL is gratefully acknowledged (DFG LA 2804/12-1). The funding sources had no impact on the study design.

Competing interests
The authors declared no potential conflicts of interest with respect to the research, authorship, and/or publication of this article.

Availability of data and materials
Not applicable.

ORCID iDs
Franz Marxreiter https://orcid.org/0000-0002-5187-4344

Jan Kassubek https://orcid.org/0000-0002-7106-9270

Supplemental material
Supplemental material for this article is available online.

References
1. Wenning GK, Geser F, Krismer F, *et al.* The natural history of multiple system atrophy: a prospective European cohort study. *Lancet Neurol* 2013; 12: 264–274.
2. Low PA, Reich SG, Jankovic J, *et al.* Natural history of multiple system atrophy in the USA: a prospective cohort study. *Lancet Neurol* 2015; 14: 710–719.
3. Gilman S, Wenning GK, Low PA, *et al.* Second consensus statement on the diagnosis of multiple system atrophy. *Neurology* 2008; 71: 670–676.
4. Stankovic I, Quinn N, Vignatelli L, *et al.* A critique of the second consensus criteria for multiple system atrophy. *Mov Disord* 2019; 34: 975–984.
5. Lehericy S, Vaillancourt DE, Seppi K, *et al.* The role of high-field magnetic resonance imaging in Parkinsonian disorders: pushing the boundaries forward. *Mov Disord* 2017; 32: 510–525.

6. Chelban V, Bocchetta M, Hassanein S, *et al.* An update on advances in magnetic resonance imaging of multiple system atrophy. *J Neurol* 2018; 266: 1036–1045.
7. Liu X, Wang N, Chen C, *et al.* Swallow tail sign on susceptibility map-weighted imaging (SMWI) for disease diagnosing and severity evaluating in parkinsonism. *Acta Radiol* 2020; 62: 234–242.
8. Meijer FJ, Steens SC, van Rumund A, *et al.* Nigrosome-1 on susceptibility weighted imaging to differentiate Parkinson's disease from atypical Parkinsonism: an in vivo and ex vivo pilot study. *Pol J Radiol* 2016; 81: 363–369.
9. Halliday GM, Holton JL, Revesz T, *et al.* Neuropathology underlying clinical variability in patients with synucleinopathies. *Acta Neuropathol* 2011; 122: 187–204.
10. Hoffmann A, Ettle B, Battis K, *et al.* Oligodendroglial A-synucleinopathy driven neuroinflammation in multiple system atrophy. *Wiley Online Library* 2018; 29: bpa12678–396.
11. Dexter DT, Carayon A, Javoy-Agid F, *et al.* Alterations in the levels of iron, ferritin and other trace metals in Parkinson's disease and other neurodegenerative diseases affecting the basal ganglia. *Brain* 1991; 114: 1953–1975.
12. Kassubek J. MRI-based neuroimaging. *Curr Opin Neurol* 2018; 31: 425–430.
13. Lambrecht V, Hanspach J, Hoffmann A, *et al.* Quantitative susceptibility mapping depicts severe myelin deficit and iron deposition in a transgenic model of multiple system atrophy. *Exp Neurol* 2020; 329: 113314.
14. Sun H, Walsh AJ, Lebel RM, *et al.* Validation of quantitative susceptibility mapping with Perls' iron staining for subcortical gray matter. *Neuroimage* 2015; 105: 486–492.
15. Pyatigorskaya N, Sanz-Morère CB, Gaurav R, *et al.* Iron imaging as a diagnostic tool for Parkinson's disease: a systematic review and meta-analysis. *Front Neurol* 2020; 11: 366.
16. Sjöström H, Granberg T, Westman E, *et al.* Quantitative susceptibility mapping differentiates between parkinsonian disorders. *Parkinsonism Relat Disord* 2017; 44: 51–57.
17. Mazzucchi S, Frosini D, Costagli M, *et al.* Quantitative susceptibility mapping in atypical Parkinsonisms. *Neuroimage Clin* 2019; 24: 101999.
18. Fedeli MP, Contarino VE, Siggillino S, *et al.* Iron deposition in Parkinsonisms: a quantitative susceptibility mapping study in the deep grey matter. *Eur J Radiol* 2020; 133: 109394.
19. Postuma RB, Berg D, Stern M, *et al.* MDS clinical diagnostic criteria for Parkinson's disease. *Movement Disord* 2015; 30: 1591–1601.
20. Berg D, Postuma RB, Adler CH, *et al.* MDS research criteria for prodromal Parkinson's disease. *Movement Disord* 2015; 30: 1600–1611.
21. Goetz CG, Tilley BC, Shaftman SR, *et al.* Movement Disorder Society-sponsored revision of the Unified Parkinson's Disease Rating Scale (MDS-UPDRS): scale presentation and clinimetric testing results. *Movement Disord* 2008; 23: 2129–2170.
22. Goetz CG, Poewe W, Rascol O, *et al.* Movement Disorder Society Task Force report on the Hoehn and Yahr staging scale: status and recommendations. *Mov Disord* 2004; 19: 1020–1028.
23. Herrler J, Liebig P, Gumbrecht R, *et al.* Fast online-customized (FOCUS) parallel transmission pulses: a combination of universal pulses and individual optimization. *Magn Reson Med* 2021; 85: 3140–3153.
24. Eckstein K, Dymerska B, Bachrata B, *et al.* Computationally efficient combination of multi-channel phase data from multi-echo acquisitions (ASPIRE). *Magn Reson Med* 2018; 79: 2996–3006.
25. Li W, Avram AV, Wu B, *et al.* Integrated Laplacian-based phase unwrapping and background phase removal for quantitative susceptibility mapping. *NMR Biomed* 2014; 27: 219–227.
26. Isensee J and Hucho T. TRP channels, methods and protocols. *Methods Mol Biology* 2019; 1987: 111–124.
27. Wu B, Li W, Guidon A, *et al.* Whole brain susceptibility mapping using compressed sensing. *Magn Reson Med* 2012; 67: 137–147.
28. Li W, Wang N, Yu F, *et al.* A method for estimating and removing streaking artifacts in quantitative susceptibility mapping. *Neuroimage* 2015; 108: 111–122.
29. Chen Y, Liu S, Wang Y, *et al.* STrategically Acquired Gradient Echo (STAGE) imaging, part I: creating enhanced T1 contrast and standardized susceptibility weighted imaging and quantitative susceptibility mapping. *Magn Reson Imaging* 2018; 46: 130–139.
30. Jenkinson M and Smith S. A global optimisation method for robust affine registration of brain images. *Med Image Anal* 2001; 55: 143–156.

31. Jenkinson M, Bannister P, Brady M, *et al.* Improved optimization for the robust and accurate linear registration and motion correction of brain images. *Neuroimage* 2002; 17: 825–841.

32. Reiter E, Mueller C, Pinter B, *et al.* Dorsolateral nigral hyperintensity on 3.0T susceptibility-weighted imaging in neurodegenerative Parkinsonism. *Mov Disord* 2015; 30: 1068–1076.

33. Ravanfar P, Loi SM, Syeda WT, *et al.* Systematic review: Quantitative Susceptibility Mapping (QSM) of brain iron profile in neurodegenerative diseases. *Front Neurosci* 2021; 15: 618435.

34. Zhang Y, Wei H, Cronin MJ, *et al.* Longitudinal data for magnetic susceptibility of normative human brain development and aging over the lifespan. *Data Brief* 2018; 20: 623–631.

35. Du G, Lewis MM, Sica C, *et al.* Distinct progression pattern of susceptibility MRI in the substantia nigra of Parkinson's patients. *Mov Disord* 2018; 33: 1423–1431.

36. Guan X, Xuan M, Gu Q, *et al.* Regionally progressive accumulation of iron in Parkinson's disease as measured by quantitative susceptibility mapping. *NMR Biomed* 2017; 30: e3489.

37. Lancione M, Cencini M, Costagli M, *et al.* Diagnostic accuracy of Quantitative Susceptibility Mapping in Multiple System Atrophy: the impact of echo time and the potential of histogram analysis. *NeuroImage Clin* 2022; 34: 102989.

38. Sood S, Urriola J, Reutens D, *et al.* Echo time-dependent quantitative susceptibility mapping contains information on tissue properties. *Magn Reson Med* 2017; 77: 1946–1958.

39. Zhou D, Cho J, Zhang J, *et al.* Susceptibility underestimation in a high-susceptibility phantom: dependence on imaging resolution, magnitude contrast, and other parameters. *Magn Reson Med* 2017; 78: 1080–1086.

40. Faul F, Erdfelder E, Buchner A, *et al.* Statistical power analyses using G*Power 3.1: tests for correlation and regression analyses. *Behav Res Methods* 2009; 41: 1149–1160.

41. Voelker MN, Kraff O, Goerke S, *et al.* The traveling heads 2.0: multicenter reproducibility of quantitative imaging methods at 7 Tesla. *Neuroimage* 2021; 232: 117910.